



# CHORUS

This is the accepted manuscript made available via CHORUS. The article has been published as:

## Spin freezing into a disordered state in $\text{CaFeTi}_{2}\text{O}_{6}$ synthesized under high pressure

X. Li, W. M. Xu, M. A. McGuire, Y. Cho, M. C. Downer, Y. Wan, X. Y. Li, Z. Y. Li, Q. Cui, J.-G. Cheng, J. B. Goodenough, and J.-S. Zhou

Phys. Rev. B **98**, 064201 — Published 3 August 2018

DOI: [10.1103/PhysRevB.98.064201](https://doi.org/10.1103/PhysRevB.98.064201)

# Spin freezing into a disordered state in $\text{CaFeTi}_2\text{O}_6$ synthesized under high pressure

X. Li<sup>1</sup>, W.M. Xu<sup>2</sup>, M. A. McGuire<sup>3</sup>, Y. Cho<sup>4</sup>, M. C. Downer<sup>4</sup>, Y. Wan<sup>5</sup>, X.Y. Li<sup>1</sup>, Z.Y. Li<sup>1</sup>, Q. Cui,<sup>6</sup> J.-G. Cheng<sup>6</sup>, J. B. Goodenough<sup>1</sup>, J.-S. Zhou<sup>1\*</sup>

<sup>1</sup> Materials Science and Engineering Program, Department of Mechanical Engineering, University of Texas at Austin, Austin, Texas 78712, USA

<sup>2</sup> School of Physics and Astronomy, Tel Aviv University, 69978 Tel Aviv, Israel

<sup>3</sup> Materials Science and Technology Division, Oak Ridge National Laboratory, Oak Ridge, Tennessee, 37831, USA

<sup>4</sup> Department of Physics, University of Texas at Austin, Austin, Texas 78712 USA

<sup>5</sup> Rudolf Peierls Centre for Theoretical Physics, University of Oxford, Oxford OX1 3NP, United Kingdom

<sup>6</sup> Beijing National Laboratory for Condensed Matter Physics and Institute of Physics, Chinese Academy of Sciences, Beijing 100190, China

## Abstract

Double perovskites exhibit a variety of interesting phenomena due to numerous combinations of cation orderings and distortions.  $\text{CaMnTi}_2\text{O}_6$  and  $\text{CaFeTi}_2\text{O}_6$  are the only two discovered double perovskites that have the columnar type A-site ordering associated with the  $a^+a^+c^-$  titling system. The former perovskite, synthesized recently, has a polar structure below  $T_c$  and shows an unusual ferroelectricity. The latter, while synthesized decades ago, received less investigation. Here, we have synthesized  $\text{CaFeTi}_2\text{O}_6$  under high pressure and carried out thorough characterizations through measurements of X-ray powder diffraction (XRD), second harmonic generation (SHG), DC and AC magnetization, Mössbauer spectra, resistivity, thermoelectric power, and specific heat. Although the structural refinement of the XRD pattern cannot distinguish two possible tetragonal phases, SHG measurements help to rule out the possibility of a polar structure observed in  $\text{CaMnTi}_2\text{O}_6$ . Fitting the paramagnetic susceptibility to a Curie-Weiss law gives a negligible Weiss constant. The weak exchange interaction gives way to a dipole-dipole interaction and single-ion anisotropy. An anomaly at 1.2 K in the specific heat is too broad for a magnetic transition, but suggestive of a spin-ice-like state as in the pyrochlores. Mössbauer spectroscopy shows two distinct iron sites, as expected for the crystal structure. Both sites are occupied by high-spin  $\text{Fe}^{2+}$  as indicated by the isomer shift. The sharply different temperature dependence of the quadrupole splitting at the two

iron sites can be well explained based on the local structural distortions from the refinement of XRD patterns. The line broadening associated with long spin-relaxation times is observed at 6 K as the spin freezing transition is approached from high temperatures.

## Introduction

Double perovskites with the general formula  $AA'BB'O_6$  can accommodate a variety of cation ordering at both A and B sites [1], which host complex orbital/spin orderings, colossal magnetoresistance [2], charge transfer and disproportionation [3], and multiferroic properties [4,5]. There are a total of 15 tilting systems to describe the corner-sharing  $BO_6$  octahedral tilting in the subgroups as the symmetry lowers from the cubic structure ( $Pm-3m$ ) of simple perovskite  $ABO_3$  [6]. However, only four Glazer tilting systems  $a^+a^+a^+$ ,  $a^0b^+b^+$ ,  $a^0b^+b^-$  and  $a^+a^+c^-$  have been known so far to create the crystallographic non-equivalence of the A-site cations in double perovskites or the A-site ordered perovskites, where +, -, and 0 denote the  $BO_6$  octahedra along a given axis tilt on the same direction (in-phase), on opposite direction (out-of-phase), and no tilt, respectively. Among these tilting systems,  $a^+a^+a^+$  tilting produces a number of double perovskites with highly distorted crystal structure; but no compound has been discovered experimentally with the  $a^0b^+b^+$  or  $a^0b^+b^-$  tilting system.  $CaMnTi_2O_6$  (CMTO) and  $CaFeTi_2O_6$  (CFTO) are the two rare cases that have the  $a^+a^+c^-$  tilting system [7]. Leinenweber and Parise synthesized CFTO under high pressure in the 1990s and studied the crystal structure [8,9]. The X-ray diffraction pattern of CFTO can be fitted best by the structural model with a non-polar space group  $P4_2/nm$  shown in the inset of Fig. 1. The  $a^+a^+c^-$  tilting system creates a columnar ordered A-site coordination where the tetrahedral  $Fe(1)O_4$  and square-planar  $Fe(2)O_4$  are placed alternately along the  $c$  axis. The structure remains stable for temperatures down to 84 K as revealed by the convergent beam electron diffraction (CBED) and high-resolution transmission electron microscopy (HREM) [10]. Following up the initial report of CFTO synthesized under high pressure, Reiff *et al.* carried out measurements of magnetic susceptibility and Mössbauer spectroscopy on CFTO [11]. The magnetic susceptibility indicated the high-spin  $Fe^{2+}$  at all Fe sites and no long-range magnetic order down to 4.2 K. The Mössbauer spectroscopy confirmed high-spin  $Fe^{2+}$  at both the tetrahedral and coplanar sites. Moreover, a slow paramagnetic relaxation rate was found at the two  $Fe^{2+}$  sites.

The same columnar A-site ordered perovskite structure has been found recently in CMTO synthesized under pressure [7]. In contrast to CFTO,  $Mn^{2+}$  at the coplanar site in CMTO

stays off the plane. It is the order-disorder transition of this displacement that induces a ferroelectric transition at  $T_c$  [4]. A type-C magnetic ordering occurs at  $T_N \approx 8$  K. The difference of orbital occupation between  $\text{Fe}^{2+}$  and  $\text{Mn}^{2+}$  and/or the displacement at the coplanar site of  $\text{MnO}_4$  may contribute to the absence of magnetic ordering in CFTO. Another possibility is that the lowest temperature in the previous measurement on CFTO is not low enough to pick up the ordering signal. More interestingly, a recent DFT calculation predicted that CFTO is a half metal [12]. To test this interesting prediction and to verify whether CFTO indeed undergoes a magnetic ordering, we revisited the double perovskite CFTO. In this paper, we have synthesized the double perovskite CFTO and measured specific heat and AC susceptibility with a  $^3\text{He}$  and a dilution refrigerator. The results reveal an interesting spin freezing into a disordered state at  $T \approx 1.2$  K. We have also studied the temperature dependences of the crystal and magnetic structures by X-ray diffraction and Mössbauer spectroscopy and also its transport properties.

### **Experimental details**

The polycrystalline CFTO sample of this study was synthesized under 15 GPa and 1200 °C in a Walker-type multianvil module (Rockland Research Co.) from a mixture of  $\text{CaTiO}_3$  (Alfa, 99%+) and  $\text{FeTiO}_3$  (Alfa, 99.8%) with a molar ratio of 1:1 as the starting material. The whole assembly for high-pressure and high-temperature (HPHT) synthesis was described in a previous publication [13]. A small piece from the high-pressure product was ground into a fine powder that was examined by powder X-ray diffraction (XRD) at room temperature with a Philips X'pert diffractometer (Cu  $K_\alpha$  radiation). The structural study at different temperatures was performed with a PANalytical X'pert diffractometer (Cu- $K_{\alpha 1}$  radiation) with an Oxford PheniX cryostat at Oak Ridge National Laboratory. Structural parameters were obtained by refining the XRD patterns with the software FULLPROF [14]. Transport data were collected with a Physical Property Measurement System (PPMS) and a homemade apparatus. Specific heat was measured in a PPMS with a dilution refrigerator. DC magnetization was measured with a superconducting quantum interference device (MPMS) magnetometer. A high-quality single crystal of  $\text{Dy}_2\text{Ti}_2\text{O}_7$  was grown by the floating-zone method with an image furnace [15]; it has been used as a reference material for the spin ice phase. Measurement of

second harmonic generation (SHG) microscopy was performed with a Ti: Sapphire laser, centered at 780 nm wavelength with 76 MHz repetition rate and 150 fs pulse width. The *p*-polarized laser was incident at an angle of 45° and *p*-polarized SH light (390 nm) was collected by a photo-multiplier tube (PMT). The CMTO was synthesized under 7 GPa and 1200°C in the Walker-type multianvil module, which is used as a reference for ferroelectric material with nearly the same crystal structure as CFTO in the SHG measurement. Mössbauer spectra were recorded in the temperature range 6–300 K with a L-He cryostat. The source used was a commercial 10 mCi <sup>57</sup>Co(Rh) point source (0.5mm×0.5 mm). All spectra were fitted by the least squares procedure from which the hyperfine interaction parameters of the various spectral components and their relative abundance were derived. The isomer shift (IS) cited is relative to alpha iron metal at ambient temperature. The AC magnetic susceptibility down to 0.3 K was measured in a <sup>3</sup>He refrigerator with the mutual induction method; an AC current of 1.117 kHz in the excitation was used, which generates a field 13 Oe. For the setup of AC susceptibility at  $T > 2$  K in the PPMS, an AC current of 0.1 kHz, 1 kHz and 10 kHz was used, which generates a field of 10 Oe. Output signal across two oppositely wound secondary coils was picked up with a Stanford Research SR830 lock-in amplifier.

## Results

### 1. Structural characterizations

The main panel of Fig. 1 shows the pattern of powder XRD and the result of Rietveld refinement; the XRD pattern of the as-made CFTO sample can be fit very well with a structural model of the double perovskite with space group  $P4_2/nmc$  (No. 137). The lattice parameters of  $a = 7.4997(5)$  Å,  $c = 7.5533(7)$  Å from the refinement are in good agreement with the values reported previously [8]. We have also tried to fit the pattern with a polar structure,  $P4_2mc$  (No. 105) and a similar fitting goodness has been obtained. It seems difficult to determine whether CFTO is with either the non-polar  $P4_2/nmc$  or polar  $P4_2mc$  symmetry simply based on the powder XRD data. SHG microscopy is a good way to probe asymmetry in the crystal structure because SHG is sensitive to small structural distortion and is suppressed in a centrosymmetric structure.

Fig. 2 shows a side-by-side comparison of the SHG micrographs on the polished surfaces of CFTO and CMTO. The granular features are related to randomly oriented grains in the polycrystalline samples. In general, surfaces of crystals could become sources of weak SHG. However, compared to the bulk generated SHG, the surface generated SHG is much weaker and nearly temperature independent within a small range of temperature variation. In Fig. 2, we compare SHG intensities at room temperature and 200 °C. At room temperature, the SHG from CMTO was two orders of magnitude higher than that from CFTO. At 200 °C, the averaged SHG intensity of CMTO was decreased by a factor of 4, while that of CFTO remained almost unchanged. **These observations support that CMTO is ferroelectric and adopts a polar structure  $P4_2mc$  below a Curie temperature [7]; whereas the weak temperature-independent SHG for CFTO are only coming from the sample surface and CFTO is not ferroelectric at room temperature.**

Based on the non-polar model, the refinement results (see in Table I) give detailed information of local structure. The Ca-O polyhedra are irregular with ten Ca-O distances ranging from 2.321 Å to 2.721 Å; an averaged  $\langle \text{Ca-O} \rangle$  bond lengths 2.546 Å is very close to the ionic radius sum of  $\text{Ca}^{2+}$  and  $\text{O}^{2-}$ .  $\text{Fe}^{2+}$  ions occupy two different sites, a tetrahedral site and a square-planar site. The bond length 2.062 Å of Fe(1)-O at the tetrahedral sites and 2.072 Å for Fe(2)-O at the square-planar sites have been obtained with  $\text{Fe}^{2+}$  at centers of tetrahedral and coplanar coordination, which are close to the expected bond lengths in this double perovskite structure.

High-quality XRD patterns have also been obtained down to 20 K, which allow us to refine the structural parameters at different temperatures. As shown in Fig. 3(a), the lattice parameter  $a$  and cell volume  $V$  decrease monotonically with decreasing temperature whereas  $c$  exhibits a shallow minimum at  $T \sim 150$  K. Fig. 3(b) shows interesting changes of local interatomic distance and bond angles. The Fe(1)-O bond length at room temperature is slightly smaller than that reported by Reiff *et al* [11]. Like the temperature dependence of the  $c$  axis, the Fe(1)-O bond length also undergoes a shallow minimum at  $T \sim 150$  K. In contrast, the O-Fe(1)-O bond angles of  $\alpha$  and  $\beta$  as defined in Fig. 1 monotonically decreases with temperature. The refinement results also

give a slightly smaller Fe(2)-O bond length than that from Reiff *et al.* [11] and no obvious temperature dependence within the range of error bars.

## 2. Magnetic properties

The top panel of Fig. 4(a) displays the temperature dependence of DC magnetic susceptibility  $\chi(T)$  for CFTO under  $\mu_0 H = 0.1$  T. The zero-field cooling (ZFC) and field cooling (FC) curves diverge below  $T_f = 6$  K. The inverse paramagnetic susceptibility  $\chi^{-1}(T)$  plotted in the inset of Fig. 4(a) can be well fitted to a Curie-Weiss (CW) law in the temperature range  $6 \text{ K} < T \leq 400 \text{ K}$  with fitting parameters of effective moment  $\mu_{\text{eff}} = 5.6(1) \mu_B/\text{Fe}^{2+}$  and Weiss constant  $\theta_{\text{CW}} \approx 0$  K. The obtained  $\mu_{\text{eff}}$  is slightly larger than the spin-only value of  $4.9 \mu_B$  for high-spin  $\text{Fe}^{2+}$ , which could be related to the presence of a small amount of  $\text{Fe}^{3+}$  as discussed in the result of thermoelectric power measurement below. A  $\mu_{\text{eff}} \approx 5.5 \mu_B/\text{Fe}^{2+}$  has also been obtained by Reiff *et al.* [11]. However, a sharp upper turn in their susceptibility data at  $T < 30$  K indicates some magnetic impurities in the sample whereas the  $\chi(T)$  of our sample shows the Curie-Weiss behavior with nearly an identical Weiss constant to 1.8 K. A  $\theta_{\text{CW}} \approx 0$  K indicates that the net effect to the Weiss molecular field from the spin-spin superexchange interaction and the dipole-dipole interaction between  $\text{Fe}^{2+}$  is about to vanish.

The splitting between the ZFC and FC of  $M(T)$  curves at  $T < T_f \approx 6$  K might mean either a canted AF ordering or a spin freezing in a spin glass system. We have further measured the DC magnetization under different magnetic fields. As displayed in the bottom panel of Fig. 4(a), the cusp in the ZFC curve is broadened and the  $T_f$  is shifted to lower temperatures as the field is increased. Both features are typical of spin freezing behavior [16]. Moreover, we have measured the spin relaxation effect of the ZFC magnetization at different temperatures in Fig. 4(b). In these measurements, the magnetization measurement starts after (1) cooling the sample down to different temperatures near  $T_f$  and (2) applying the field  $H = 0.1$  T. The value of 100% relaxation is defined as the magnetization of FC at a given temperature. The magnetization relaxes quickly as temperature is close to  $T_f$  from below; while it shows no relaxation at 10 K because the



magnetization of ZFC and FC are overlapped above  $T_f$ . The behavior is also typical for a spin glass or freezing spin system.

The temperature dependence of AC susceptibility  $\chi_{AC}(T)$  in Fig. 5(a) provides additional information about the magnetic state at low temperatures. Due to the limitation of the  $^3\text{He}$  refrigerator, we can only obtain  $\chi_{AC}(T)$  within 0.3-2.2 K at the frequency of 1117 Hz. With the PPMS, we have performed the measurement of AC susceptibility from 1.8 to 30 K at different frequencies (see Fig. 5(b)). Corresponding to the temperature where FC and ZFC curves of DC susceptibility in Fig. 4(a) split,  $\chi_{AC}(T)$  shows a hump which moves to higher temperatures as the frequency increases. This observation confirms the spin-glass behavior at  $T_f \approx 6$  K. A similar feature of  $\chi_{AC}(T)$  has been reported for the spin-ice material  $\text{Dy}_2\text{Ti}_2\text{O}_7$  at a higher temperature [17].

In order to further reveal the thermodynamics of the spin system, we have measured specific heat under high magnetic fields with high precision down to 0.05 K.  $C_p(T)$  in Fig. 6(a) exhibits a broad hump at  $T \approx 1.2$  K, which is slightly lower but close to the anomaly seen in the AC magnetic susceptibility in Fig. 5. After subtracting the lattice contribution  $C_{\text{lattice}}$ , which can be obtained by extrapolating the Debye-Einstein fitting from the high-temperature  $C_p(T)$  to low temperatures, the black curve in Fig. 6(a), we are able to show in Fig. 6(b) that the  $C_{\text{mag}}$  is much broader than a  $\lambda$ -shape transition characteristic of a magnetic ordering. An integration of  $C_{\text{mag}}/T$  in Fig. 6(c) over a temperature range covering the transition gives a total entropy change on crossing the transition,  $\Delta S \approx 5.5$  J/mol K, which is only about half of the expected value  $R \ln(2S+1) = 13.4$  J/mol K for a  $S = 2$  system. Moreover, the hump of  $C_{\text{mag}}(T)$  at  $T \approx 1.2$  K is suppressed slightly and moved to higher temperatures under a magnetic field; but the total entropy change remains more or less constant. This observation suggests a ferromagnetic ordering at 1.2 K. On the other hand, however, a similar result has been reported on  $\text{Dy}_2\text{Ti}_2\text{O}_7$  which exhibits a spin-ice state at 1.2 K [18].

Mössbauer spectroscopy (MS) is a local probe to detect local structural distortions through the hyperfine interactions, the valence state of MS active cations, and spin dynamics. Fig. 7 shows the high-resolution MS data on CFTO. The essential features of

MS at room temperature are consistent with that obtained by Reiff *et al.*[11]. However, an obvious difference between results from the two studies can be found at low temperatures, especially at  $T < 10$  K. No detailed analysis was provided in the MS study by Reiff *et al* [11]. The double perovskite structure provides two crystallographic sites, tetrahedral and coplanar, for the  $\text{Fe}^{2+}$  cation. The MS at room temperature can be fit easily with two Fe centers, a smaller quadrupole splitting (QS) of 0.41 mm/s and a larger QS of 2.80 mm/s. The isomer (IS) shift of both centers is about 1 mm/s, typical for high-spin  $\text{Fe}^{2+}$  [19]. Table II summarizes QS and IS for the two Fe centers at different temperatures.

MS reflects interactions between the nucleus and the electrons that can be described by a Hamiltonian including terms of  $H_0$  (atom),  $E_0$  (electric monopole),  $M_1$  (magnetic dipole), and  $E_2$  (electric quadrupole). The chemical environment of the MS active ions in a compound can be derived from the MS. For example, the magnitude of QS indicates a deviation from a cubic field and the temperature independence of the QS generally confirms lack of orbital degeneracy and low-lying excited states. In the case of CFTO, a small QS found for Fe1 indicates that the Fe ion is at the site with a nearly cubic field, which is at the tetrahedral site. A larger QS for Fe2 places the Fe ion unambiguously at the coplanar site. Moreover, the crystal field for Fe1 at tetrahedral sites creates degenerate orbitals of  $z^2$  and  $x^2-y^2$ . The orbital degeneracy is gradually lifted due to a local structural distortion as temperature decreases, which explains the highly temperature dependent QS for Fe1. The temperature dependences of the  $\alpha$  and  $\beta$  angles at the tetrahedral site, which are resolved in the structural study of Fig. 3(b), support the argument. In contrast, the crystal field splitting at the Fe2 site makes the  $z^2$  orbital fully occupied and clearly separated from the excited state of partially occupied  $yz$  and  $zx$  orbitals. Therefore, a temperature-independent QS is expected. The MS results support these considerations. Although the line width for Fe1 looks broader than that of Fe2, the fitting results indicate the abundance of Fe1 and Fe2 is actually identical. A smaller QS at Fe1 makes the two lines nearly overlap at room temperature. The line width remains broader as two lines start to separate at low temperatures. A broader line width for Fe1 suggests some bond length splitting at the site, which is randomly distributed between the tetrahedral sites and cannot be resolved easily by X-ray diffraction.

By following the trend of QS and the line width for both centers at high temperatures, the MS data at 6 K can be fit well with a total of four lines caused by the QS at two centers plus a residual component (the green line of Fitting I in Fig. 7). Since the residual component is not close to the expectation from a spin relaxation model, we have chosen the fitting with broader line width without adding a residual component (Fitting II in Fig. 7). The fitting result rules out any possibility of spin ordering at 6 K. However, the result of significantly broader line width is consistent with a glassy spin state.

Fig. 8(a) shows the magnetization measurement over the range  $-9 \leq H \leq 9$  T at different temperatures. At  $T = 1.8$  K, the M-H hysteresis loop exhibits a small coercivity  $H_C \leq 0.1$  T and a remnant magnetization  $M_r \approx 0.2 \mu_B/\text{Fe}^{2+}$ , which is normally seen in a spin glass because changing the field at a temperature below  $T_f$  leads to a pronounced irreversible magnetization. The saturated magnetization at  $T = 1.8$  K approaches  $\sim 2.6 \mu_B/\text{Fe}^{2+}$  at 9 T and a similarly high saturation moment can be found for temperatures up to 10 K. Moreover, the broad curvature of  $M(H)$  is closer to a Brillouin function than a typical magnetization curve for a ferromagnet. The observation of non-linear  $M(H)$  curve at temperatures where a Curie-Weiss law is fulfilled indicates a nearly free spin system in CFTO. Stunningly similar magnetization curves of Fig. 8(b) have been observed in a pyrochlore  $\text{Dy}_2\text{Ti}_2\text{O}_7$ , which also has a negligibly small Weiss constant. The spin dynamics reflected in the magnetization measurement, the specific heat result, and the MS result will be discussed in the context of spin freezing into a spin disordered state in the discussion section.

### 3. Transport properties

The resistivity  $\rho(T)$  and thermoelectric power  $S(T)$  of CFTO have been measured over a broad range of temperature. Due to a high resistance of the sample pellet, which is comparable to that of the input resistance of the nanovoltmeter used in the measurement at low temperatures, reliable data of  $\rho(T)$  and  $S(T)$  in Fig. 9 can be obtained only at high temperatures. The resistivity increases monotonically with decreasing temperature, suggestive of an insulator, which is in contrast to the prediction that CFTO is a half metal [12]. In a simple insulator,  $\rho$  follows an activated T dependence of  $\rho \propto \exp(-\Delta/2k_B T)$ ,

where  $\Delta$  is the band gap. The plot of  $\ln(\rho)$  versus  $1/T$  in the inset of Fig. 9(a) shows a linear behavior; fitting the data to a line gives an energy gap of  $\Delta = 0.52$  eV. Fig. 9(b) shows a temperature independent thermoelectric power  $S$  in the temperature range 240 - 320 K, suggesting a polaronic conduction. The  $S$  fluctuates below 240 K due to an extremely high resistance in the sample. A  $S \approx 200$   $\mu\text{V/K}$  corresponds to a hole density of 0.1/formula unit based on the Heike's formula  $S = (k/e) \ln[(1 - c)/c]$  [20], which means 0.05 vacancies at either the Fe or Ca site in CFTO. Therefore, the small energy gap obtained from the conductivity measurement must be the activation energy for polarons to hop instead of a band gap in an intrinsic insulator.

## Discussion

The columnar ordered CFTO is a unique structure where the magnetic  $\text{Fe}^{2+}$  are located at a relatively isolated A site. The interatomic distance between  $\text{Fe}^{2+}$ - $\text{Fe}^{2+}$  within a chain along the  $c$  axis is 3.77 Å; the distance between chains is 5.30 Å. The shortest interatomic distance in CFTO is longer than the 3.57 Å in the pyrochlore  $\text{Dy}_2\text{Ti}_2\text{O}_7$ , which exhibits a spin-ice behavior [18]. Like the pyrochlore  $\text{Dy}_2\text{Ti}_2\text{O}_7$ , the total spin-spin interaction is negligible in CFTO as confirmed by a very small Weiss constant  $\theta \sim 0.5$  K in  $\text{Dy}_2\text{Ti}_2\text{O}_7$  and a  $\theta \approx 0$  K in CFTO. The dipole-dipole interaction and a strong single-ion anisotropy lead to the spin freezing into a spin-ice phase at 1.2 K in  $\text{Dy}_2\text{Ti}_2\text{O}_7$  [18]. The peculiar physical property of a spin-ice state is obtained mainly from the result of a specific heat measurement. The transition to a spin-ice state does not give up all the system entropy. The residual entropy is about  $(R/2) \ln(3/2)$ , which is exactly the entropy for ice first derived by Pauling [21]. The residual entropy in a spin-ice state comes from a high number of possible patterns to arrange spins while they still fulfill the ice rule, *i.e.* two-in and two-out configuration. The peak of specific heat on crossing the transition is much broader than the  $\lambda$ -shape peak for a magnetic transition. Specifically, a long tail is found on the high-temperature side. The temperature profile of  $C_{\text{mag}}(T)$  at the transition is similar to a Schottky peak. However, the first excited state lies several hundreds of Kelvin above the ground state, which rules out any possibilities for the Schottky anomaly for a two-energy system. The broad peak in a spin-ice system simply reflects the entropy change associated with freezing spins. A clear splitting between the field-cooled and

zero-field cooled of  $M(T)$  and the Curie-Weiss law behavior in the field-cooled  $M(T)$  confirm that spins are frozen into a disordered state. Due to the extremely weak spin-spin interaction, spins in the paramagnetic state act as in a free spin system described by a Brillouin function. A non-linear magnetization with high saturation moment is shown in Fig. 8(b) for a pyrochlore  $Dy_2Ti_2O_7$ .

The thermodynamics of the spin-ice state in pyrochlores helps us to understand the spin state in CFTO at low temperatures. The negligible spin-spin interactions extracted from the paramagnetic susceptibility does not lead to a magnetic ordering state down to 50 mK. Although the magnetization relaxation result and the AC susceptibility suggest a spin-glass state in CFTO at 1.2 K, the anomaly of specific heat at low temperatures indicates some entropy change due to spin ordering. However, similar to the transition to a spin-ice state, the peak of  $C_{mag}(T)$  at 1.2 K is too broad for a spin ordering. Whereas the orbital momentum is quenched at both iron sites, the spin-orbit coupling in higher orders brings in a strong single-ion anisotropy (SIA), which normally orients spins along the axis with the highest rotation symmetry [22]. In the CFTO structure, the SIA tends to align spins along the  $c$  axis because it has the highest rotation symmetry at both tetrahedral and coplanar sites. Since interatomic interactions either from the superexchange interactions or the dipole-dipole interaction is extremely weak, spins can still flip while aligned along the  $c$  axis. Moreover, the spin freezing actually starts at higher temperatures as indicated by the split of FC and ZFC magnetization curves. The partially ordered spin matrix produces a magnetic field that causes the line broadening in MS at 6 K. To our best knowledge, this paper is the first study of a spin-freezing state by MS.

In a spin-ice system, the residual entropy is due to a huge number of possible patterns for the two-in and two-out spin configuration. The missing entropy is gradually recovered under a magnetic field as spins are lined up [18]. Although a magnetization similar to that for the spin-ice system is observed in CFTO, the  $C_{mag}$  moves to higher temperatures and becomes much broader with increasing magnetic field. In this case,  $C_{mag}$ , which is only a small fraction of the lattice contribution, is spread over a broader temperature range. The fitting to the lattice contribution has a larger uncertainty at higher temperatures, which leaves no chance for us to derive a valid  $C_{mag}$  anymore.

It is important to distinguish between the spin freezing state studied here and the state of a canonical spin glass. The fundamental difference is that the spin degree of freedom is reduced in the spin freezing state; spins are aligned to the  $c$  axis in CFTO, whereas spins remain disordered in the spin-glass state. The most striking phenomenon is that the saturated magnetization in the low-temperature regime approaches  $\sim 2.6 \mu_B/\text{Fe}^{2+}$ , which is significantly larger than that of a conventional spin-glass phase.

It is also interesting to compare physical properties of CFTO with those of isostructural CMTO. The  $\text{Mn}^{2+}$  in the coplanar site in CMTO moves off the oxygen plane. While ordering of this displacement is the origin for a ferroelectric transition, it does not play a decisive role in the exchange interaction. CMTO exhibits a regular magnetic ordering at 10 K. The dramatic difference of magnetic properties between CFTO and CMTO must be related to the electronic structure in these two double perovskites. The  $z^2$  orbital has the lowest energy for  $\text{Fe}^{2+}$  or  $\text{Mn}^{2+}$  at the coplanar site. It should be noted that the common arrangement of orbital energy for ions at the coplanar site in the textbook is to place degenerate  $xy$  and  $zx$  orbitals at the lowest energy. The DFT calculation does not support this arrangement. In CMTO, the half-filled  $z^2$  orbital at the coplanar site bridges the AF superexchange interaction through the degenerate partially occupied  $e_g$  orbital at the tetrahedral site along the  $c$  axis as is illustrated in the inset of Fig. 1. In contrast, the  $z^2$  orbital at the coplanar site is fully occupied in CFTO; therefore the  $\text{Fe}^{2+}$  at the coplanar sites do not have a superexchange interaction along the  $c$  axis.

The structural framework of a columnar ordered perovskite provides a new playground where more interesting magnetic properties can be achieved by the chemical tuning of cations with partially filled orbitals at the tetrahedral and coplanar sites. It makes more sense to write the formula as  $A_2A'A''B_4O_{12}$ , where cations at different local coordination can be clearly specified. In a review paper about the A-site columnar ordered perovskites, Belik has summarized the possible cations suitable for either the tetrahedral site or the coplanar site or on both sites [5]. This chemical roadmap helps to tailor the orbital occupation at particular crystallographic sites so as to achieve the desired magnetic ground state. Research along this line would certainly provide an insight of the partially ordered spin state found in CFTO. On the negative side, since the structure requires

highly selective occupation of cations at different crystallographic sites with a fixed valence state, the global instability index (GII) is high for almost all  $A_2A'A''B_4O_{12}$  perovskites which makes high-pressure synthesis generally required and limits the availability of samples in research laboratories.

## **Conclusion**

The double perovskite  $\text{CaFeTi}_2\text{O}_6$  synthesized under high pressure and high temperature is an insulator, which is in contrast to a half-metal predicted by a DFT calculation. The SHG measurement helps to select the non-polar state among two possible structural models for the double perovskite CFTO, which cannot be distinguished easily by X-ray diffraction. The electronic configuration together with the peculiar columnar ordered structure creates a situation where both the superexchange interaction and the dipole-dipole interaction are extremely weak, which facilitates a spin freezing into a spin disordered state at low temperatures. Like the spin-ice state in pyrochlores or in the Kagome lattice, the system gives up a great portion of its entropy as spins are frozen into the spin disordered state. Spins are likely aligned on the  $c$  axis due to the strong single-ion anisotropy at the coplanar site, but the detailed spin structure remains to be determined with neutron diffraction.

\*jszhou@mail.utexas.edu

## **Acknowledgement**

This research was primarily supported by the National Science Foundation through the Center for Dynamics and Control of Materials: an NSF MRSEC under Cooperative Agreement No. DMR-1720595. JBG and MCD were supported by Welch Foundation, Houston, Texas, in USA with grant number F-1066 and F-1038. M.A.M. acknowledges support from the US Department of Energy, Office of Science, Basic Energy Sciences, Materials Sciences and Engineering Division. JGC was supported by the CAS, NSFC, and MOST (Grant Nos. 11574377, 2014CB921500, QYZDB-SSW-SLH013, XDB07020100).

## References

- [1] M. T. Anderson, K. B. Greenwood, G. A. Taylor, and K. R. Poeppelmeier, *Prog. Solid State Chem.* **22**, 197 (1993).
- [2] K.-I. Kobayashi, T. Kimura, H. Sawada, K. Terakura, and Y. Tokura, *Nature* **395**, 677 (1998).
- [3] Y. W. Long, N. Hayashi, T. Saito, M. Azuma, S. I. Muranaka, and Y. Shimakawa, *Nature* **458**, 60 (2009).
- [4] Z. Li, Y. Cho, X. Li, X. Li, A. Aimi, Y. Inaguma, J. A. Alonso, M. T. Fernandez-Diaz, J. Yan, M. C. Downer, G. Henkelma, J. B. Goodenough, and J. Zhou, *J. Am. Chem. Soc.* **140**, 2214 (2018).
- [5] A. Belik, *Dalton Trans.* **47**, 3209 (2018).
- [6] G. Burns and A. Glazer, *Space Groups for Scientists and Engineers* (Academic Press, Inc., Boston, MA, 1990).
- [7] A. Aimi, D. Mori, K. Hiraki, T. Takahashi, Y. J. Shan, Y. Shirako, J. Zhou, and Y. Inaguma, *Chem. Mater.* **26**, 2601 (2014).
- [8] K. Leinenweber and J. Parise, *J. Solid State Chem.* **114**, 277 (1995).
- [9] K. Leinenweber, J. Linton, A. Navrotsky, Y. Fei, and J. B. Parise, *Phys. Chem. Miner.* **22**, 251 (1995).
- [10] N. Yao, A. Navrotsky, and K. Leinenweber, *J. Solid State Chem.* **123**, 73 (1996).
- [11] W. M. Reiff, K. Leinenweber, and J. Parise, *Solid-State Chem. Inorg. Mater.* **453**, 387 (1997).
- [12] H. Li, S. Liu, L. Chen, C. Li, and Z. Wang, *Physica E: Low-Dimens. Syst. Nanostruct.* **69**, 133 (2015).
- [13] X. Li, J.-Q. Yan, D. J. Singh, J. B. Goodenough, and J.-S. Zhou, *Phys. Rev. B* **92**, 155118 (2015).
- [14] J. Rodriguez-Carvajal, satellite meeting on powder diffraction of the XV congress of the IUCr, Toulouse, France, 127 (1990).
- [15] Q. J. Li, L. M. Xu, C. Fan, F. B. Zhang, Y. Y. Lv, B. Ni, Z. Y. Zhao, and X. F. Sun, *J. Cryst. Growth* **377**, 96 (2013).
- [16] C. M. Soukoulis, K. Levin, and G. S. Grest, *Phys. Rev. Lett.* **48**, 1756 (1982).
- [17] J. Snyder, B. G. Ueland, J. S. Slusky, H. Karunadasa, R. J. Cava, A. Mizel, and P. Schiffer, *Phys. Rev. Lett.* **91**, 107201 (2003).
- [18] A. P. Ramirez, A. Hayashi, R. J. Cava, R. Siddharthan, and B. S. Shastry, *Nature* **399**, 333 (1999).
- [19] T. C. Gibb and N. N. Greenwood, *Mössbauer Spectroscopy* (Chapman and Hall, London, 1971).
- [20] R. R. HEIKES and W. Roland, *Thermoelectricity, Science and Engineering* (Wiley-Interscience, Inc., New York 1961).
- [21] L. Pauling, *J. Am. Chem. Soc.* **57**, 2680 (1935).
- [22] J.-S. Zhou, J. A. Alonso, A. Muoz, M. T. Fernández-Díaz, and J. B. Goodenough, *Phys. Rev. Lett.* **106**, 057201 (2011).



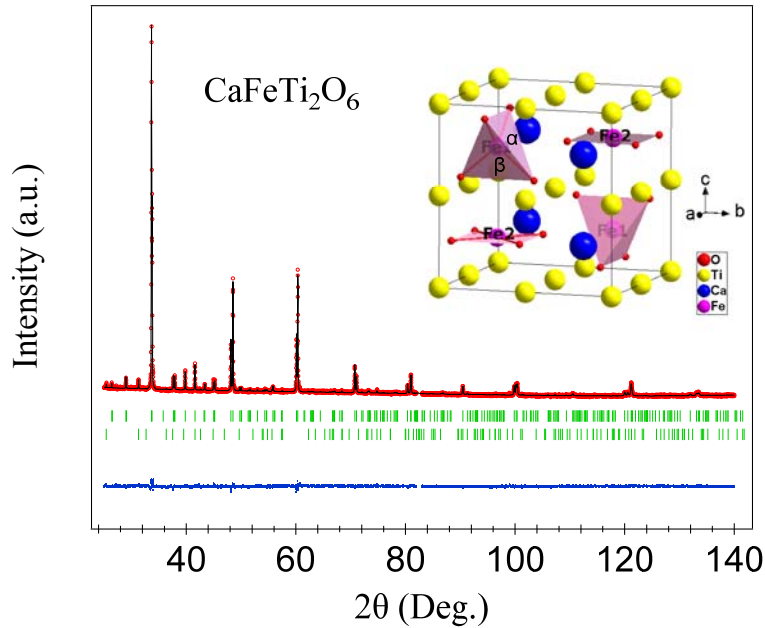


Fig. 1 (Color online) The powder XRD pattern of CFTO at room temperature the results of Rietveld refinement with the space group  $P4_2/nmc$  (No. 137): a tiny amount impurity of  $TiO_2$  ( $\sim 2\%$ ) was observed; a peak in the range of  $82^\circ$  to  $83^\circ$  from the sample holder is excluded; the insert panel shows the crystal structure of CFTO.

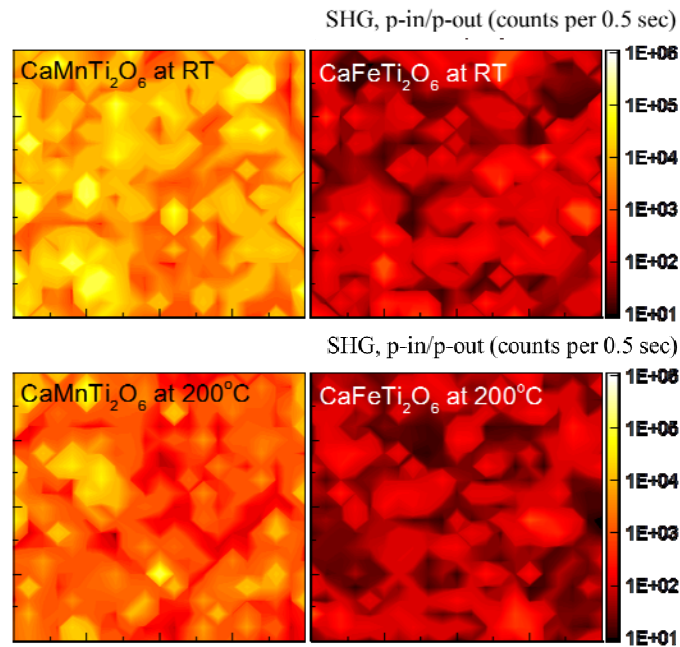


Fig. 2 (Color online) SHG micrographs on CFTO and CMTO: Top panels were measured at room temperature, and the bottom panels at  $200^\circ\text{C}$ . The average SHG of CFTO was very weak (around 170 counts at room temperature) and nearly temperature independent; whereas two orders of magnitude stronger SHG was observed on CMTO and the intensity was decreased by a factor of four with increasing temperature.

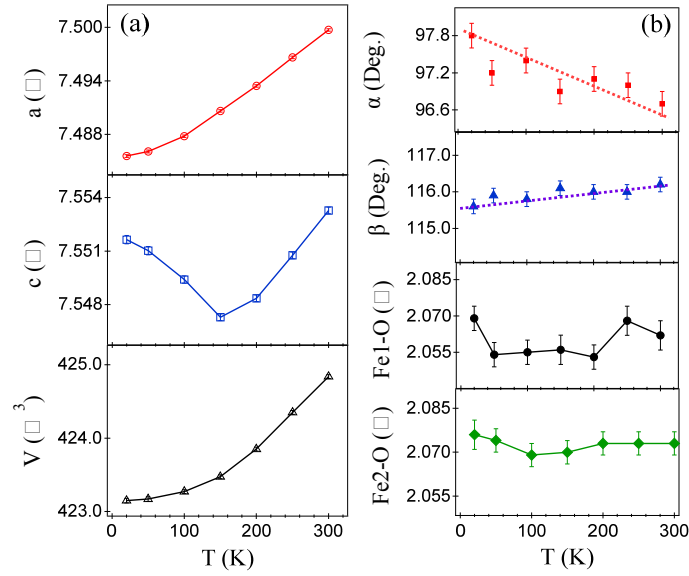


Fig. 3 (Color online) Temperature dependence of (a) lattice parameters and Volume (most error bars are smaller than symbols used in these plots), (b) local interatomic distances and bond angles in CFO.

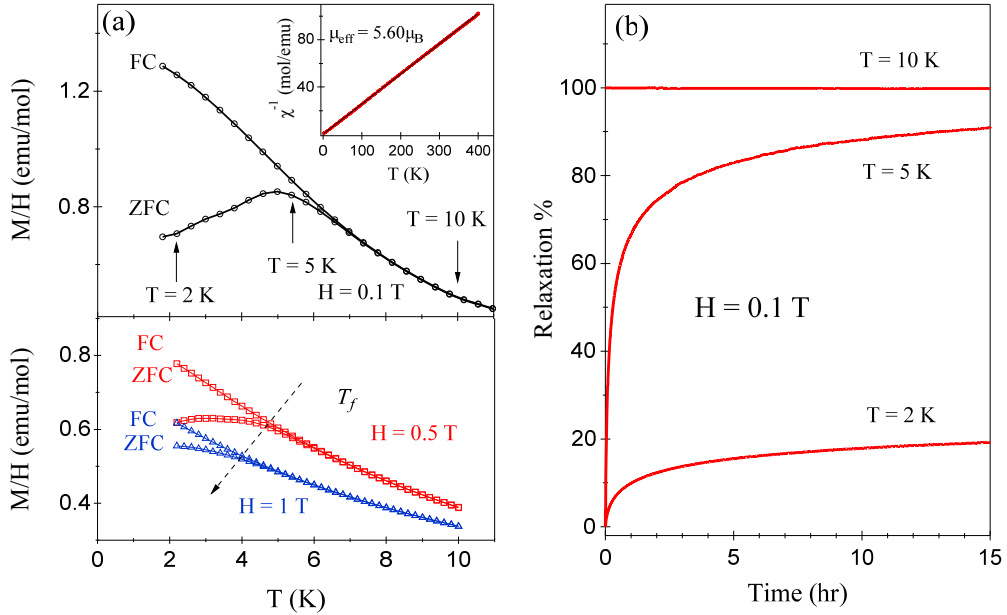


Fig. 4 (Color online) (a) Temperature dependence of DC magnetic susceptibility  $\chi$  under different magnetic fields after cooling at the same rate of 10 K/min; (b) Relaxation of the ZFC magnetization under 0.1 T at different temperatures of 2 K, 5 K and 10 K, respectively. The value of 100% corresponds to the FC curve at three temperatures.

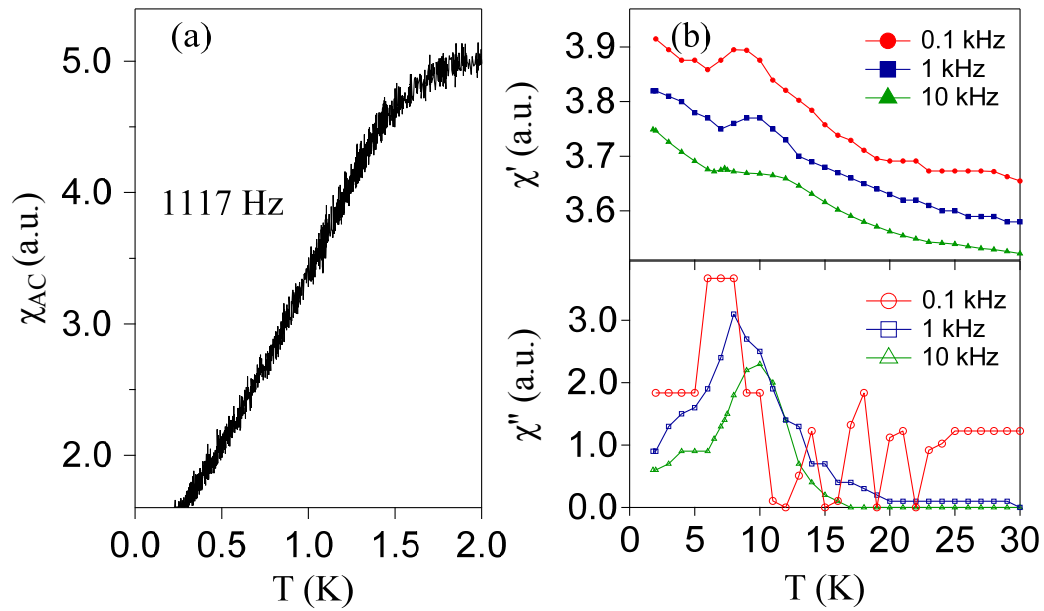


Fig. 5 (Color online) (a) Temperature dependence of AC susceptibility below 2 K measured in a  $^3\text{He}$  refrigerator. (b) Temperature dependence of AC susceptibility (real part  $\chi'$  and imaginary part  $\chi''$ ) at different frequencies from 1.8 K to 30 K of CFTO.  $\chi''$  at 0.1 kHz is noisy because the signal is too low to be picked up by the lock-in amplifier at the highest gain.

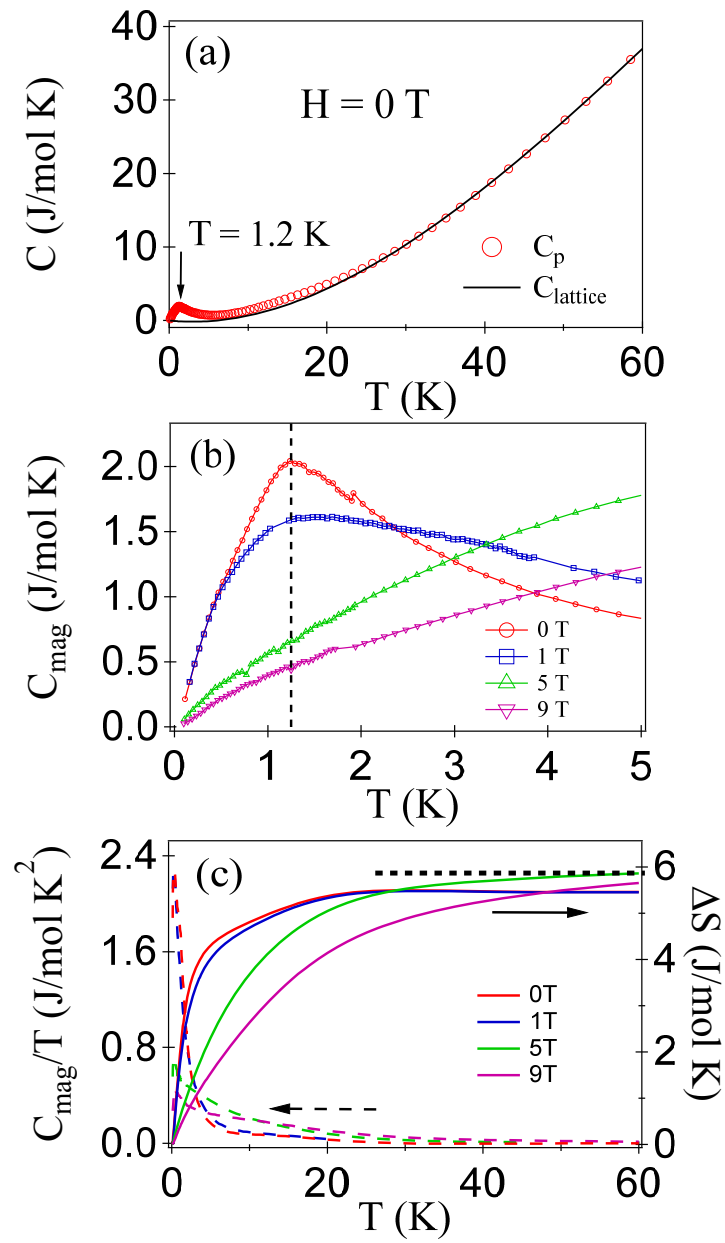


Fig. 6 (Color online) Temperature dependence of (a) specific heat  $C(T)$  at zero field; (b) magnetic specific heat  $C_{\text{mag}}(T)$  and (c) magnetic entropy  $\Delta S$  under different fields for CFTO.

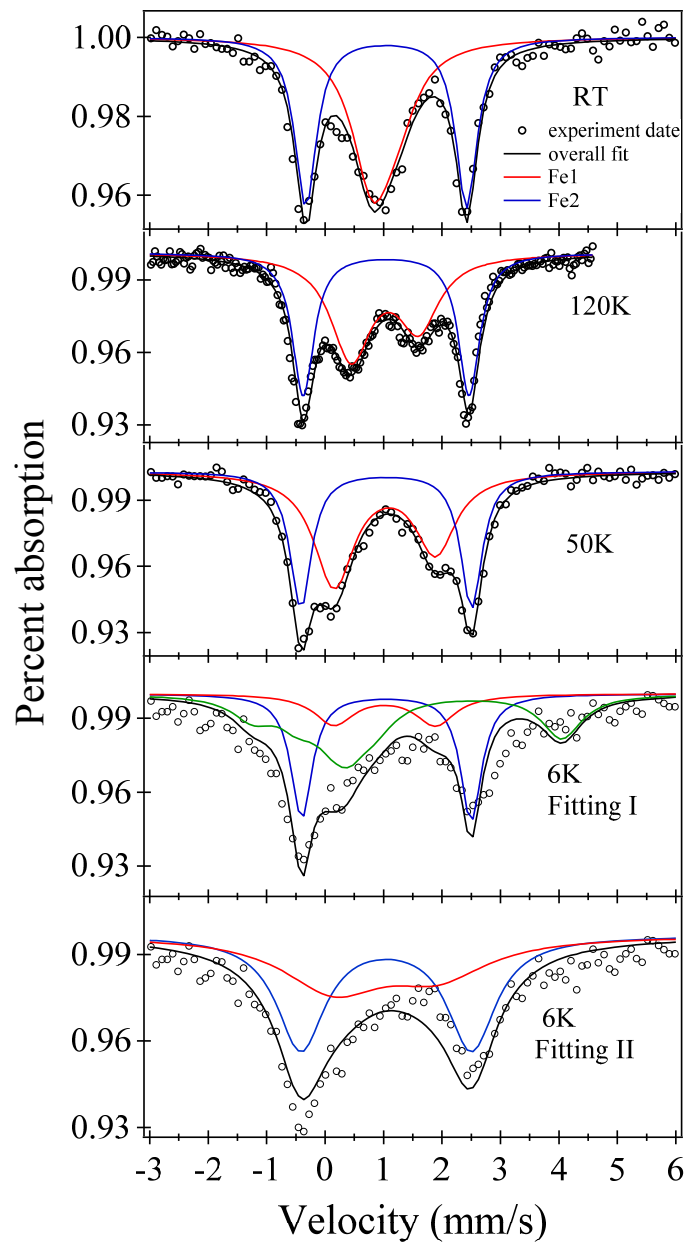


Fig. 7 (Color online) Mössbauer spectroscopy of CFTO at different temperatures. The open circles are experiment data and black solid lines are the overall fit to the data from the subcomponents shown; the red and blue solid lines are fittings for the hyperfine interactions at the tetrahedral Fe1 site and coplanar Fe2 site, respectively; the green solid line represents a residual component in addition to the contribution from QS at 6 K, see the text for detailed information about analyzing MS data.

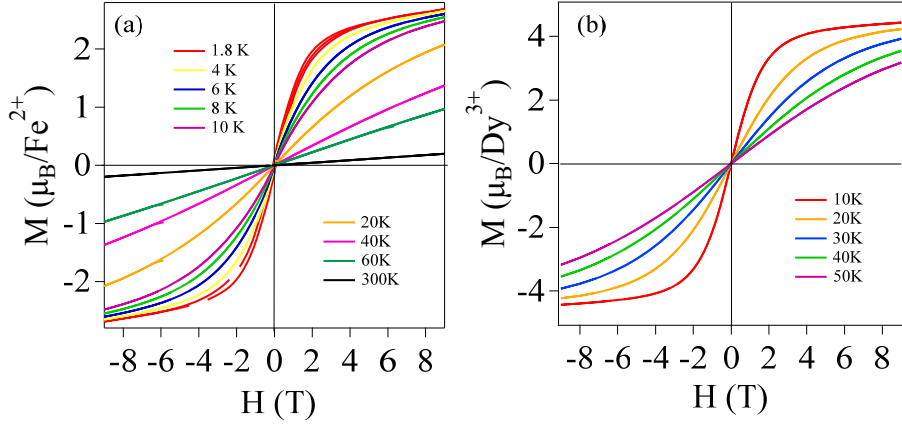


Fig. 8 (Color online) Magnetization over the range  $-9 \text{ T} \leq H \leq 9 \text{ T}$  at different temperatures for (a) CFTO; and (b)  $\text{Dy}_2\text{Ti}_2\text{O}_7$ .

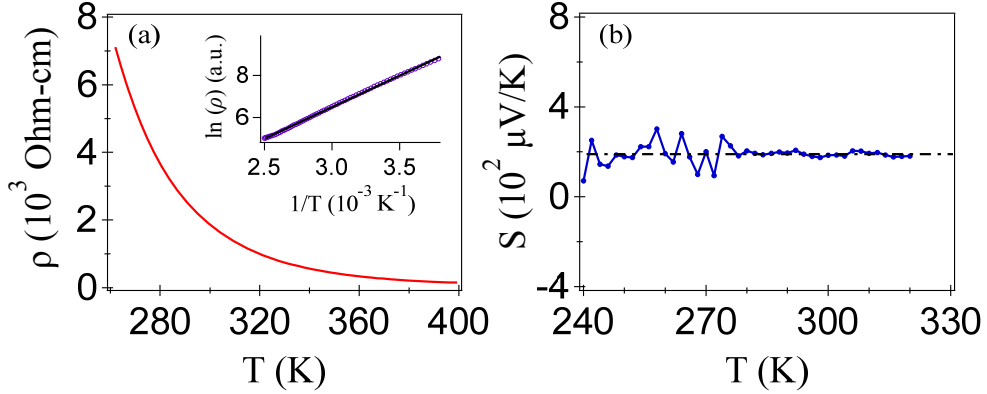


Fig. 9 (Color online) Temperature dependence of (a) resistivity  $\rho(T)$ ; and (b) thermoelectric power  $S(T)$  for CFTO.

Table I: Structural refinement of CFTO with the space group  $P4_2/nmc$  (No. 137)<sup>a</sup> at room temperature.

Atom	x	y	z	$U_{\text{iso}}$
O1 (8g)	0.2500	0.0544(10)	0.0373(9)	0.0152(9)
O2 (8g)	0.2500	0.5444(10)	0.4313(9)	0.0152(9)
O3 (8f)	0.5546(5)	0.4454(5)	0.25000	0.0152(9)
Ti (8e)	0.0000	0.0000	0.0000	0.0178(3)
Ca (4d)	0.2500	0.2500	0.2754(5)	0.0178(3)
Fe1(2b)	0.7500	0.2500	0.7500	0.0178(3)
Fe2(2a)	0.7500	0.2500	0.2500	0.0178(3)

<sup>a</sup>The lattice parameters:  $a = 7.4997(5) \text{ \AA}$ ,  $c = 7.5533(7) \text{ \AA}$  and  $V = 424.84(1) \text{ \AA}^3$ ;  $R_p = 2.75$ ,  $R_{\text{wp}} = 3.49$ ,  $R_{\text{exp}} = 2.73$  and  $\chi^2 = 1.64$ .

Table II: Experimental results of Isomer Shifts (IS) and Quadrupole Splitting (QS) from fitting Mo<sup>55</sup>ssbauer spectra at different temperatures for CFTO.

<b>Atom</b>		<b>RT</b>	<b>120 K</b>	<b>50 K</b>	<b>6 K</b>
Tetrahedral	IS (mm/s)	0.85	1.01	1.03	1.03
Fe1	QS (mm/s)	0.41	1.10	1.68	1.68
Coplanar	IS (mm/s)	1.03	1.06	1.04	1.08
Fe2	QS (mm/s)	2.80	2.84	2.99	2.90